CrystEngComm

Accepted Manuscript

This article can be cited before page numbers have been issued, to do this please use: A. Purkayastha, S. Dhar, S. P. Mondal, A. Franconetti, A. Frontera, R. Ganguly, A. Kirillov and T. K. Misra, *CrystEngComm*, 2020, DOI: 10.1039/C9CE01437C.

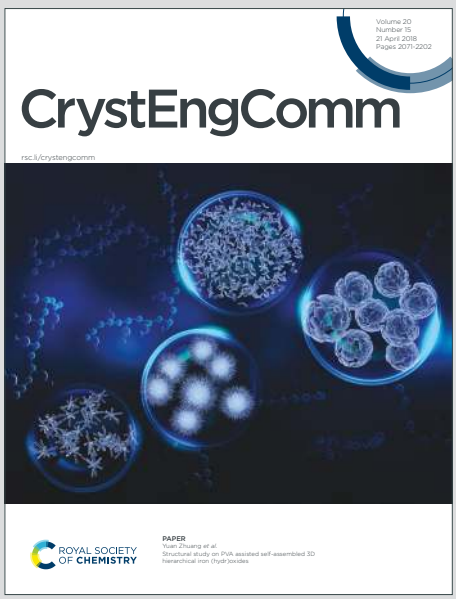

ROYAL SOCIETY OF CHEMISTRY

rsc.li/crystengcomm

View Article Online
DOI: 10.1039/C9CE01437C

ARTICLE

Metal-organic Architectures Driven by a Multifunctional 6-Aminouracil Spacer: Structures, Noncovalent Interactions, and Conductivity

Received 00th January 20xx,
Accepted 00th January 20xx

DOI: 10.1039/x0xx00000x

Atanu Purkayastha,[a] Sourav Dhar,[b] Suvra Prakash Mondal,[b] Antonio Franconetti,[c] Antonio Frontera,*[c] Rakesh Ganguly,*[d] Alexander M. Kirillov,*[e,f] Tarun Kumar Misra*[a]

Three new coordination polymers, $[Na^{I}(H_2L)(H_2O)_3]_n$ (**1**), $\{[K^{I}(H_2L)(H_2O)]_8 \cdot 13H_2O\}_n$ (**2**), and $\{[Ni^{II}Na^{I}_2(HL)_2(H_2O)_8] \cdot 6H_2O\}_n$ (**3**) were assembled from 1,3-dimethyl-5-(*p*-sulfonic-phenylazo)-6-aminouracil (H_3L) as a versatile building block. Although azo-coupling reactions generally result in simple azo-compounds, the presence of the sulfonate ($-SO_3^-$) group at the ligand frame led to the formation of the Na^{I}-1D (**1**) or K^{I}-3D (**2**) homometallic coordination polymers with different ligand coordination modes. Moreover, heterometallic Ni^{II}/Na^{I}-1D (**3**) coordination polymer was obtained while carrying the reaction of **2** with $NiCl_2 \cdot 6H_2O$. The structures of the obtained products were fully established by single crystal X-ray diffraction and confirmed by standard methods. Compounds **1** and **3** possess 1D metal-organic chains with the 2C1 topology, whereas **2** features a very complex 3D metal-organic architecture with an unprecedented topology. The computational study for molecular electrostatic potential (MEP) surface energies revealed an important finding, namely a decrease of the π-acidity of the uracil ring upon coordination and a consequent increase of the π-basicity of the phenyl-sulfonate ring, resulting in effective anti-parallel π-π stacking interactions in **1** and **2**. Finally, a semi-conductive behavior of the obtained compounds was explored using an impedance spectroscopy, revealing the very remarkable conductive properties of **1** (2.2×10^{-4} S·cm^{-1}), which is a far better conductive material than **2** (7.2×10^{-6} S·cm^{-1}) and **3** (4.8×10^{-7} S·cm^{-1}). The obtained products represent the first coordination compounds derived from H_3L. This study contributes to the design of functional coordination polymers driven by still poorly explored 6-aminouracil building blocks.

1. Introduction

Research on coordination polymers (CPs) is mainly focused on transition metal compounds because of their fascinating applications in various fields.[1,2] In contrast, CPs of s-block metal ions are investigated to a significantly lower extent.[3] However, such compounds, especially those incorporating physiological metal ions (e.g., Na^+, K^+), can exhibit different types of structural motifs, properties and applications which, in some cases, can be advantageous in respect to toxicity, solubility in water, and bioavailability. The design of organic spacers or linkers for engineering and assembling new coordination polymers is also an important step.[1,4] Apart from having a pre-defined skeleton, such building blocks are generally ornamented with the functional –COOH or $–SO_3H$ groups which provide a coordination versatility and potential water solubility.

Azo derivatives with sulfonate ($-SO_3^-$) or sulfonic acid (SO_3H) groups are particularly attractive compounds in the fields of biomedical research,[5-9] analytical chemistry[10] and materials science.[11] Coordination polymers based on s-block metals and sulfonated monoazo building blocks have been reported,[12–17] including materials with interesting gas sorption and anion exchange properties.[16] Kennedy *et al.*[13–15] have demonstrated a supramolecular architecture of s-block metal sulfonated monoazo dyes by investigating a role of cations and position of sulfonate group in the aryl ring. The sulfonate based CPs with advanced solid-state electrical/ion/proton-conductivity and biological properties have also been documented.[18–27]

In recent years, we have been particularly interested in exploring the chemistry of uracil derivatives[28] given their importance in the fields of bioactive molecules and drug design. In particular, the coordination chemistry of azo-uracil derivatives is mainly centered at 1,3-dimethyl-5-(aryazo)-6-aminouracil.[28] Keeping the 1,3-dimethyl-6-aminouracil moiety intact, we have recently developed a new series of azo-uracils

[a] Department of Chemistry, National Institute of Technology Agartala, Tripura 799046, India; E-mail: tkmisra.chem@nita.ac.in / tkmisra70@yahoo.com
[b] Department of Physics, National Institute of Technology Agartala, Tripura 799046, India
[c] Departamento de Química, Universitat de les Illes Balears, Crta. de Valldemossa 07122, Spain; E-mail: toni.frontera@uib.es
[d] Division of Chemistry & Biological Chemistry, Nanyang Technology University, Singapore 639798; E-mail: rganguly@ntu.edu.sg
[e] Centro de Química Estrutural, Instituto Superior Técnico, Universidade de Lisboa, Av. Rovisco Pais, 1049-1005, Lisbon, Portugal; E-mail: kirillov@tecnico.ulisboa.pt
[f] Research Institute of Chemistry, Peoples' Friendship University of Russia (RUDN University), 6 Miklukho-Maklaya st., Moscow, 117198, Russian Federation

†Electronic Supplementary Information (ESI) available: IR spectra (Figures S1–S3), TGA (Figure S4), connectivity mode of the ligand (Figure S5), NMR (Figures S6–S10), and UV-vis (Figures S11–S13) spectra, as well as bond lengths and angles for **1**–**3** (Tables S1–S6). CCDC numbers 1902620, 1902621, and 1902619 for **1**–**3**, respectively. See DOI: 10.1039/x0xx00000x

by changing substituent at the phenyl ring. Metal complexes bearing such ligands have also been prepared and shown a variety of weak intermolecular interactions such as H-bonding, π-π stacking, lp-π and CH/NH-π interactions. Interestingly, in some cases, the conductivity of a material could also be tuned by a type of noncovalent interactions.[18–27] These interactions have already been explored on 1,3-dimethyl-5-(aryazo)-6-aminouracils and their nickel(II) systems and have shown a predominate effect on substituent at the phenyl ring.[28] In addition, such organic blocks can be applied for the synthesis of coordination polymers.[28i]

Following the above background, in this report we have attempted the synthesis of new homo- and heterometallic coordination polymers based on s-block metal nodes (Na, K) and optional transition metal (Ni) centers. Interestingly, during the synthesis of a sulfonated monoazo ligand (1,3-dimethyl-5-(*p*-sulfonic-phenylazo)-6-aminouracil, H_3L, Scheme 1), a coupling reaction between *p*-diazobenzenesulfonic acid and 1,3-dimethyl-6-aminouracil in the presence of different bases (*i.e.*, NaOH or KOH) has been attempted. Instead of generating H_3L, we have isolated its derivatives, $[Na^I(H_2L)(H_2O)_3]_n$ (**1**) and $\{[K^I(H_2L)(H_2O)]_8{\cdot}13H_2O\}_n$ (**2**) (Scheme 1), two novel homometallic Na(I) and K(I) coordination polymers that bear new H_2L^- blocks generated in *situ*. In addition, a heterometallic coordination polymer $\{[Ni^{II}Na_2^I(HL)_2(H_2O)_8]{\cdot}6H_2O\}_n$ (**3**) has also been assembled. Hence, this study provides the full characterization of the obtained compounds **1**–**3**, describes their spectroscopic, structural and topological features, solution behavior as well as theoretical analysis. In fact, DFT analysis of the π-π stacking interactions in **1** and **2** including the MEP and NCI plot computational tools has been performed. Finally, the electric conductivity of the obtained compounds has been investigated, revealing a particularly remarkable conductive behavior of compound **1**.

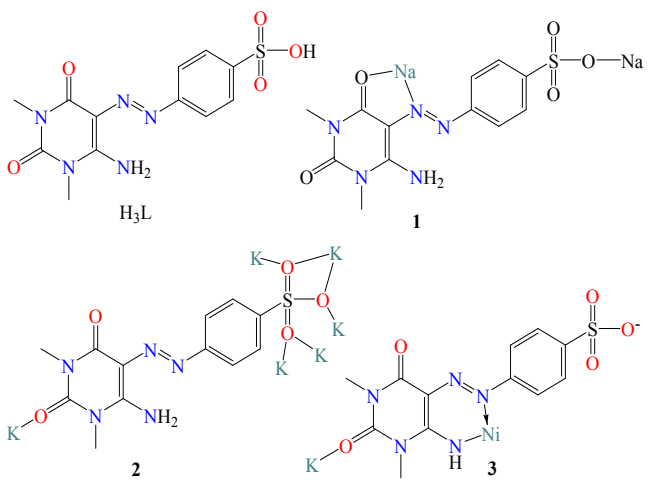

Scheme 1. Molecular structure of H_3L and simplified representation of derived coordination compounds **1**–**3**. For simplicity, only one μ_5-mode of H_2L^- is shown in **2**.

2. Experimental section

Materials and methods

Reagent grade chemicals including 1,3-dimethyl-6-aminouracil, *p*-aminobenzenesulfonic acid (p-$H_2NC_6H_4SO_3H$, sulfanilic acid), nickel(II) chloride hexahydrate ($NiCl_2{\cdot}6H_2O$), hydroxides of sodium and potassium and sodium nitrite were purchased from commercial sources and used without further purification. Solvents used for synthesis and spectroscopic studies were of Analytical Reagent (A.-R.) grade. Silver paste was purchased from Ted Pella Inc. (USA).

Melting points were determined on a Labtech Digital melting point apparatus. IR spectra (4000-400 cm^{-1}) were recorded on a Perkin Elmer (RX-1 FT-IR) spectrophotometer as KBr pellets. NMR (^1H at 500 MHz and ^{13}C at 125 MHz) spectra were recorded using DMSO-D_6 solutions and a JEOL DELTA2 spectrometer. Shimadzu UV-Vis 1800 spectrophotometer was used for measuring electronic spectra. TGA analysis of the compounds was performed on a Perkin Elmer made Diamond TG/DTA tool. Impedance Analyzer (Keysight, E4990A) was used to measure the conductivity at room temperature and in the frequency range of 20 Hz – 1 MHz. Elemental analyses were conducted with a Perkin Elmer 2400 series-II analyzer.

Synthesis and analytical data for coordination polymers 1–3

$[Na^I(H_2L)(H_2O)_3]_n$ (1)

Sodium(I) derivative of 1,3-dimethyl-5-(*p*-sulfonic-phenylazo)-6-aminouracil (H_3L) was isolated while adjusting a solution pH with NaOH of the coupling reaction between *p*-diazobenzenesulfonic acid and 1,3-dimethyl-6-aminouracil. In brief, a diazotized solution of *p*-aminobenzenesulfonic acid (1.211 g, 7.0 mmol) in aqueous HCl (30 mL, 4 M) was subjected to coupling with 1,3-dimethyl-6-aminouracil (1.112 g, 6.46 mmol) in acetic acid-water mixture (20 mL, 1:3 v/v) at 0-5 ºC. The resulting solution pH was then adjusted to ~5-6 with a 1 M aqueous solution of NaOH, which generated a yellow precipitate. This was filtered off, washed with cold water, and dried in an air-oven at 60 ºC. The dried product was dissolved in DMF and set for crystallization, resulting in the formation of crystals within a week. Yellow needle shape crystals, yield: 82%; m.p. 295±2 °C; FT-IR (KBr, selected bands, υ cm^{-1}). 3561 and 3455 (br, ν(O-H) and ν(N-H)), 1701 (^{2}C=O), 1636 (^{4}C=O), 1520 (C=C), 1464 (N=N), 1363 & 1118 (C-N), 1229 & 1029 (ν_{as} and ν_s(S=O)); ^1H NMR (DMSO-D_6, δ ppm): 11.78 (br, 1H, -NH-), 8.70 (s, 1H, =NH), 7.70–7.68 (d, phenyl-H), 7.63-7.60 (m, phenyl-H), 3.37 & 3.25 (ss, N-CH_3); ^{13}C NMR (125 MHz, DMSO-D_6, δ ppm): 27.80 (N-CH_3), 29.19 (N-CH_3), 110.11(CH), 119.96 (CH), 126.46 (C), 147.30 (C), 148.91 (C), 149.73 (C), 151.95 (C=O), 159.15(C=O). Anal. Calcd. for $C_{12}H_{18}N_5NaO_8S$: C, 34.47; H, 4.37; N, 16.86, Found: C, 35.05; H, 4.81; N, 16.56.

$\{[K^I(H_2L)(H_2O)]_8{\cdot}13H_2O\}_n$ (2)

Potassium(I) coordination polymer **2** was prepared following the procedure described for **1** but using KOH instead of NaOH. Yellow needle crystals, yield: 74%; m.p. 295±2 °C; FT-IR (KBr, selected bands, υ cm^{-1}). 3451 and 3342 (br, ν(O-H) and ν(N-H)), 1710 (^{2}C=O), 1624 (^{4}C=O), 1530 (C=C), 1462 (N=N), 1362 & 1123 (C-N), 1206 & 1034 (ν_{as} and ν_s(S=O)); ^1H NMR (DMSO-D_6, δ ppm): 11.77 (br, 1H, -NH-), 8.74 (s, 1H, =NH), 7.66–7.65 (d, phenyl-H),

View Article Online DOI: 10.1039/C9CE01473C

7.60−7.58 (m, phenyl -H), 3.35 & 3.23 (ss, N-CH_3); ^{13}C NMR (125 MHz, DMSO-D_6, δ ppm): 27.76 (N-CH_3), 29.13 (N-CH_3), 110.13(CH), 119.88 (CH), 126.42 (C), 147.35 (C), 148.93 (C), 149.76 (C), 151.92 (C=O), 159.14(C=O). Anal. Calcd. for $C_{96}H_{138}N_{40}K_8O_{61}S_8$: C, 33.90; H, 4.06; N, 16.48, Found: C, 33.29; H, 3.79; N, 16.24.

{[$Ni^{II}Na^{I}_2(HL)_2(H_2O)_8$]·$6H_2O$}$_n$ (3)

Compound **2** (0.1 mmol) was dissolved in methanol (10 mL). To the solution, a solid sodium acetate (CH_3COONa, 1.0 mmol) was added in one portion. The reaction mixture was refluxed at 80 °C for 1 h under constant stirring. Then, a solid nickel(II) chloride (0.05 mmol) was added in one portion, causing an immediate change of the color of the reaction mixture from yellow to reddish brown. The final reaction mixture was refluxed for additional 2 h. Thereafter, it was cooled down to room temperature and kept undisturbed for crystallization. After a few days, a good quantity of crystals was formed. Red block crystals, yield 78 %; m.p. >300 °C, FT-IR (KBr, selected bands, υ cm^{-1}) 3472 and 3364 (br, ν(O-H) and ν(N-H)), 1709 (^{2}C=O), 1665 (^{4}C=O), 1566 (C=N), 1457 (N=N), 1314 & 1125 (C-N), 1195 & 1036 (ν_{as} and ν_s(S=O)); ^{1}H NMR (DMSO-D_6, δ ppm): 7.51 (s, phenyl-H), 4.62 (s, 1H, -NH), 3.32 & 3.17 (s, N-CH_3); ^{13}C NMR (125 MHz, DMSO-D_6, δ ppm): 28.10 (N-CH_3), 29.02 (N-CH_3), 118.02(CH), 123.58 (CH), 125.73 (C),141.12(C) 146.64(C), 149.37(C), 151.89 (C=O), 158.25(C=O). Anal. Calcd. for $C_{24}H_{50}N_{10}NiNa_2O_{24}S_2$: C, 27.92; H, 4.85; N, 13.57, Found: C, 27.65; H, 5.08; N, 13.70.

X-ray crystallography data collection and structure refinement

Single crystals of compounds **1** and **2** were generated by recrystallization from their solutions in DMF. Single crystals of **3** were obtained directly from the reaction mixture. A suitable crystal of each sample was selected and subjected to intensity data collection at 100(2) K, using a Bruker AXS Kappa APEX-II diffractometer equipped with a CCD area detector and graphite monochromatic MoKα radiation (λ = 0.71073 Å). Cell refinement and data reduction was performed with Bruker SAINT[29] software package and absorption effects were corrected using SADABS.[30] The structures were solved with Olex2[31] and refined with Bruker SHELXL Software Package.[32] In the course of structural solution and refinement, the space groups $P2_1/c$ with Z = 4 for **1**, C2/c with Z = 2 for **2**, and P-1 with Z = 1 for **3** were used. All the structures were solved by direct methods or Patterson maps to locate the heavy atoms, followed by difference maps for the light, non-hydrogen atoms. All the non-hydrogen atoms were refined with anisotropic thermal parameters. A summary of the crystallographic data collection and structural parameters of **1**–**3** is listed in Table 1. It is noteworthy to mention that for half a molecule of **2** (asymmetric unit), the K1 atom has an occupancy of 1.0, while the K2 and K3 atoms have an occupancy of 0.5. Hence, the overall occupancy for K is 2.0 per asymmetric unit, leading to four potassium ions in the molecule. Since it was not possible to see clear electron-density peaks in difference maps which would correspond with acceptable locations for various water H atoms in **1** and **2**, the refinement was completed with no allowance for these H atoms in the models.

Topological analysis

To get further insight into the crystal structures and packing patterns of **1**-**3**, we performed their topological analysis by applying the concept of the simplified underlying net.[33,34] The underlying nets were generated by omitting all the terminal ligands and reducing all the bridging ligands to the corresponding centroids, maintaining their connectivity with metal atoms.

Computational methods

The geometries of the compounds in this study were computed at the M06-2X/def2-TZVP level of theory using the crystallographic coordinates. For all the calculations, we have used the GAUSSIAN-09 program.[35] The Grimme's dispersion[36] correction as implemented in GAUSSIAN-09 program was also applied, since it is adequate for the evaluation of noncovalent interactions where dispersion effects like σ-hole interactions are relevant. The basis set superposition error for the calculation of interaction energies has been corrected using the counterpoise method.[37] The NCIplot[38] isosurfaces have been used to characterize noncovalent interactions. They correspond to both favorable and unfavorable interactions, as differentiated by the sign of the second density Hessian eigen value and defined by the isosurface color. The color scheme is a red-yellow-green-blue scale with red for ρ^+_{cut} (repulsive) and blue for ρ^-_{cut} (attractive).

Conductivity measurements

The low frequency electrical conductivity of the solid samples of **1**–**3** was evaluated at room temperature by preparing cylindrical pellets of the compounds with a diameter of 10 mm and a thickness of 3 mm.[39] Both sides of the pellet were uniformly painted with a thin layer of silver paste to enhance the contact between the pellet and the electrodes. The conductivity was then measured by using Impedance Analyzer in the frequency range of 20Hz – 1MHz at room temperature.

3. Results and discussion

Synthesis

View Article Online
DOI: 10.1039/C9CE01437C

Table 1. Crystallographic data and structure refinement for compounds **1**–**3**.

Empirical formula	$C_{12}H_{18}N_5NaO_8S$ (1)	$C_{24}H_{36}N_{10}K_2O_{15.25}S_2$ (2)	$C_{24}H_{50}N_{10}NiNa_2O_{24}S_2$ (3)
Formula weight	415.36	850.95	1031.55
Temperature/K	100(2)	100(2)	100(2)
Crystal system	monoclinic	monoclinic	triclinic
Space group	$P2_1/c$	C2/c	P -1
a/Å	7.7666(7)	35.2528(6)	8.1407(3)
b/ Å	10.5350(9)	15.7804(3)	8.7295(3)
c/ Å	20.5005(17)	13.0890(2)	15.6983(5)
α/°	90	90	78.8978(11)
β/°	90.853(3)	109.9540(10)	79.5625(10)
γ/°	90	90	88.0006(11)
Volume/ Å^3	1677.2(3)	6844.3(2)	1076.60(6)
Z	4	8	1
ρ_{cal} g/cm^3	1.645	1.652	1.591
μ/mm^{-1}	0.276	0.486	0.664
F(000)	864	3536	538
Crystal/size/mm^3	0.08 x 0.12 x 0.18	0.02 x 0.04 x 0.28	0.06 x 0.10 x 0.12
Radiation	MoKα (λ=0.71073)	MoKα (λ = 0.71073)	MoKα (λ=0.71073)
2θ range for data collection/°	4.34 - 56	2.341 - 30.987	4.76 – 62.22
Index ranges	-10 ≤ *h* ≤10, -13 ≤ *k* ≤13, -26≤ *l* ≤27	-51 ≤ *h* ≤ 50, -22 ≤ *k* ≤ 22, -14 ≤ *l* ≤ 18	-11≤ *h* ≤ 11, -12 ≤ *k* ≤ 12, -22 ≤ *l* ≤ 22
Reflections collected	3993	59393	24096
Independent reflections	3491 [R_{int} = 0.1285]	10864 [R_{int} = 0.0646]	6860 [R(int) = 0.0350]
Goodness - of – fit on F^2	1.106	1.062	1.029
Final R indexes[I≥2σ(I)]	R_1 = 0.0604, wR_2 = 0.1285	R_1 = 0.0474, wR_2 = 0.0960	R_1 = 0.0373, wR_2 = 0.0860
Final R indexes [all data]	R_1 = 0.0767, wR_2 = 0.1392	R_1 = 0.0830, wR_2 = 0.1163	R_1 = 0.0479, wR_2 = 0.0920
Largest diff.peak/hole/e Å^{-3}	0.527/-0.569	0.826/-0.541	0.80/-0.43

Aiming at the synthesis of a new sulfonated monoazo ligand (1,3-dimethyl-5-(p-sulfonic-phenylazo)-6-aminouracil, H_3L, Scheme 1), we attempted a coupling reaction between p-diazobenzenesulfonic acid and 1,3-dimethyl-6-aminouracil in the presence of different bases (i.e., NaOH or KOH) for adjusting pH. Instead of generating H_3L, we isolated two new homometallic Na(I) and K(I) coordination polymers formulated as $[Na^I(H_2L)(H_2O)_3]_n$ (**1**) and $\{[K^I(H_2L)(H_2O)]_8{\cdot}13H_2O\}_n$ (**2**) (Scheme 1), which bear the H_2L^- blocks generated in situ. Thus, the presence of –COOH[28i] or $–SO_3H$ groups at diazobenzene framework may lead to Na(I) or K(I) CPs of azo-derivatives depending on a base used (NaOH or KOH). Moreover, a heterometallic Ni(II)-Na(I) coordination polymer, $\{[Ni^{II}Na_2^I(HL)_2(H_2O)_8]{\cdot}6H_2O\}_n$ (**3**), was formed when reacting compound **2** with $NiCl_2{\cdot}6H_2O$ in the presence of sodium acetate in MeOH. All the obtained compounds **1**–**3** were characterized by standard methods in the solid state (FT-IR spectroscopy, elemental and TGA analyses, and single crystal X-ray diffraction) and in the solution (UV-vis and NMR spectroscopy). Despite the generation of products **1**–**3** was not fully expected, our results are well reproducible, lead to the same organic functionality in all compounds, and contribute to the exploration of a new multifunctional building block (H_3L) for the *in situ* synthesis of coordination polymers with interesting structural and functional properties. Besides, the obtained products represent the first examples of coordination compounds derived from the present type of 6-aminouracil spacer, as confirmed by a search of the Cambridge Structural Database.

FT-IR spectra and thermogravimetric analysis of 1–3

The FT-IR spectra **1**–**3** are displayed in Figures S1–S3 (ESI), while the selected bands and their assignment are given in the experimental section. In **1** and **2**, the four characteristic bands for the $\nu_{C=O}$ (two), $\nu_{C=C}$, and $\nu_{N=N}$ vibrations appear at usual positions and are comparable with the reported values for related free ligands,[28a,e] indicating that they are in the form of

azo derivatives of uracil in the solid state. In **3**, these bands are in positions typical for nickel(II) derivatives.[28d,g] All the compounds feature two additional bands in the 1229-1029 cm^{-1} region, which can be assigned to asymmetric and symmetric νO=S=O vibrations.[40]

Thermogravimetric analysis (TGA) of **1–3** was performed in the 30−1040 °C range with a heating rate of 5 °C/min (Figure S4, ESI). After dehydration (~90-125 °C), the compounds show thermal stability (~250-310 °C) before undergoing a multistage decomposition. The residual weights of the sample correspond to Na_2O (exp. 15.90%, calcd. 14.9%) for **1**, $4K_2O$ (exp. 10.45%, calcd. 11.07%) for **2** and a mixture of NiO+Na_2O (exp. 16.44%, calcd. 13.10%) for **3**. From the dehydration/decomposition temperature, it is quite evident that CP **3** has highest thermal stability than the other two compounds.

Crystal structure and topology

Crystal structures of the compounds **1**−**3** with atom numbering schemes are displayed in Figures 1–3, respectively. Bond lengths and angles are listed in Tables S1–S6 (ESI). Compounds **1** and **2** are homometallic 1D and 3D coordination polymers of Na(I) and K(I), respectively, wherein 1,3-dimethyl-5-(*p*-sulfonate-phenylazo)-6-aminouracil (H_2L^-) acts as a building block. Sulfonate group (SO_3^-) behaves as a linker at one end, while another linking functionality is N_{azo} and/or O_{uracil} of the main ligand. In **1** (Figure 1), the H_2L^- acts as a μ-linker *via* the monodentate sulfonate-O and the bidentate (N_{azo},O_{uracil}) functionalities, resulting in the formation of a tooth-like 1D metal-organic chain (Figure 4A). The six-coordinate Na1 center adopts a distorted octahedral environment filled by two O and one N donors from two H_2L^- moieties and three terminal H_2O ligands. The Na-OH_2 distances [Na(1)-O(6), 2.355(4) Å; Na(1)-O(7), 2.390(3) Å; Na(1)-O(8), 2.284(4) Å] are comparable to the related compounds.[28g] In **1**, the Na1-$O_{sulfonate}$ distance [Na(1)-O(3^i), 2.368(4) Å] is quite short for such a type of compounds.[12,41] The chelation of H_2L^- to Na(1) occurs through a bidentate (N_{azo},O_{uracil}) site; a bite angle is 58.56°. Herein, the coordination of azo-N to Na(1) is quite unusual [Na1−N2, 3.025(3) Å]. The uracil-O and sulfonate-O donors are located in opposite sites around the Na(1) center and make a nearly linear angle, [O(2)-Na(1)-O(3^i), 169.12(14)°]. The azo bond length [N1=N2, 1.274(4) Å] is slightly longer than the reported one for similar ligand systems.[28] The C=O bond [C7-O2, 1.240(5) Å] is longer than the C4-O1 [1.241(5) Å] bond and the free uncoordinated ligand values,[28] indicating a coordination of the C=O group through C7-O2 bond to Na1 in **1**. There are various hydrogen bonds involving H_2O ligands, uracil and sulfonate oxygen atoms and uracil-NH_2 group. Uracil and aromatic moiety of H_2L^- possess an almost planar E conformation around the azo functionality (the corresponding torsion angle is ca. −174°). The uracil moiety shows the dihedral angles of ca. 26 and 6° with the metal coordination plane and the phenyl ring, respectively.

In contrast to **1**, the structure of $\{[K^I(H_2L)(H_2O)]_8{\cdot}13H_2O\}_n$ (**2**) is significantly more complex and shows a 3D metal-organic network (Figures 2 and 5A). There are three crystallographically distinct K(I) atoms, namely K1 with full occupancy and K2 and K3 with half occupancy. Per asymmetric unit, there are also two H_2L^- moieties that act as μ_4- and μ_5-spacers, and one μ-H_2O and one terminal H_2O ligands. The bonding environment around each type of K(I) is different. The K1 atom is eight-coordinate and its coordination sphere bears six O-donors coming from five H_2L^- moieties, one μ-H_2O and a terminal H_2O ligand (Figure 2A). The six-coordinate K2 atom features a distorted octahedral environment that is taken by two terminal H_2O ligands and four O-donors coming from four H_2L^- spacers (Figure 2B). The K3 atom is eight-coordinate and its coordination sphere is composed of six O-donors from four H_2L^- spacers and two μ-H_2O ligands. The μ_4-H_2L^- spacer interconnects four K atoms (2K1, K2, K3) and acts as a tetradentate ligand with a sulfonate group adopting a μ_3-bridging tridentate mode (Figure S5A). The μ_5-H_2L^- moiety interlinks five K centers (3K1, K2, K3) and acts as a heptadentate ligand with a sulfonate group adopting

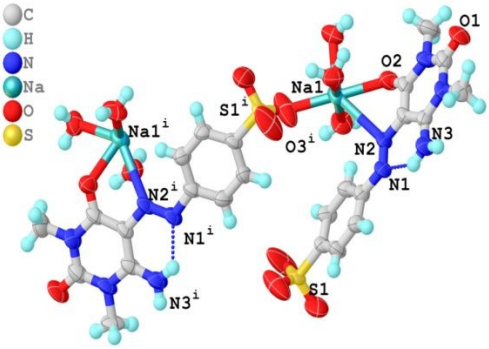

Figure 1. ORTEP view of compound **1** (50% probability ellipsoids; symmetry code: [i]2-x, -½+y, ½-z).

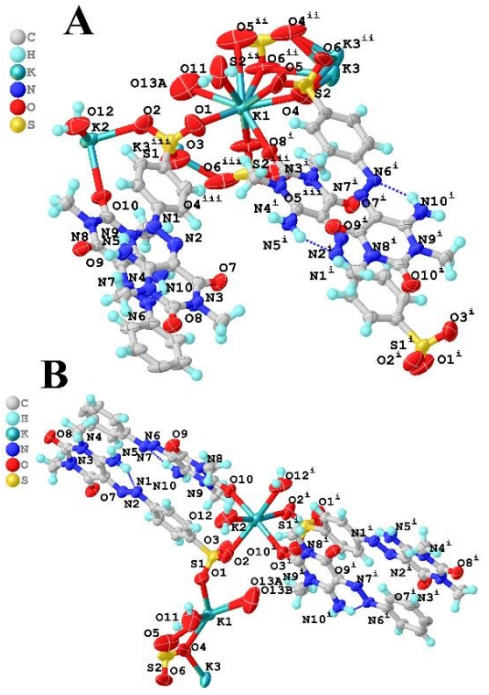

Figure 2. ORTEP view of compound **2** with over all coordination about (**A**) K1 and (B) K2 and K3 (50% probability ellipsoids; symmetry codes: [i]x, 1-y, -1/2+z; [ii]1/2-x, 1/2+y, 3/2-z; [iii]-x,+y,3/2-z). For clarity, disordered atoms and crystallization H_2O are not shown.

a μ_4-bridging hexadentate mode (Figure S5B). Such a multiple binding of K atoms by the H_2L^- spacers gives rise to a generation

of a very intricate 3D metal-organic framework (Figure 5A). Despite similarity in uracil moiety binding to a metal atom, unlike in **1**, the sulfonate group of H_2L^- in **2** uses its three O-atoms for bonding to K(I) centers. The K–$O_{sulfonate}$ distances vary in the 2.73–3.19 Å, which are much longer than the Na–$O_{sulfonate}$ distance in **1**. In both **1** and **2**, one of the azo-N (attached to a phenyl ring) interacts with the $–NH_2$ group of uracil fragment through H-bonding. In **2**, the azo (-N=N-) bond length of 1.282(2) Å is comparable with that of the free ligand.[28g]

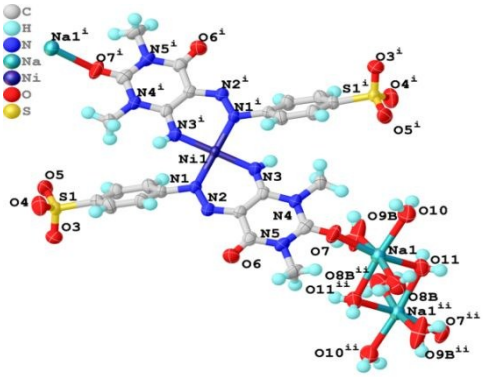

Figure 3. ORTEP view of compound **3** (50% probability ellipsoids, Symmetry codes: [i]1- x, 1- y, 2-z; [ii]1-x, -y, 1-z) (For clarity disorder and crystal water molecules are deleted)

Compound $\{[Ni^{II}Na_2^{I}(HL)_2(H_2O)_8]\cdot 6H_2O\}_n$ (**3**) is a heterometallic Ni(II)/Na(I) 1D coordination polymer (Figures 3 and 6A), which is composed of the $[Ni^{II}(HL)_2]^{2-}$ and $[Na_2^{I}(\mu\text{-}H_2O)_2(H_2O)_6]^{2+}$ units. The four-coordinate Ni1 center adopts a square planar geometry with a $\{NiN_4\}$ environment, which is filled by four N donors from two chelating HL^{2-} ligands. The $[Ni^{II}(HL)_2]^{2-}$ units are further interlinked by the $[Na_2^{I}(\mu\text{-}H_2O)_2(H_2O)_6]^{2+}$ blocks through the uracil-O atoms. Within the disodium(I) blocks, the Na1 atoms are six-coordinate and feature a distorted octahedral $\{NaO_6\}$ geometry, which is maintained by three terminal H_2O ligands, two μ-H_2O linkers, and one uracil-O donor. Unlike in **1** and **2**, the sulfonate groups of HL^{2-} remain uncoordinated in **3**. Within $[Ni(HL)_2]^{2-}$, the Ni-N(amino-NH) and Ni-N(azo–N) bond lengths are comparable with literature data.[28g] The azo bond (-N=N-) length of 1.2944(17) Å is larger than the value in the free azo ligand[28a] and **2**. The coordination of uracil-O(7) to the Na center can be understood comparing two exo-cyclic >C=O bond lengths present in the uracil moiety. The >C=O group [C4-O7, 1.2181(18) Å] which is coordinated to Na1 has a shorter distance than that of the uncoordinated functionality [C6-O6, 1.232(2) Å].

To explore the metal-organic network in **1–3**, topological analysis of the simplified underlying nets was performed.[33,34] Compound **1** reveals a 1D metal-organic network (Figure 4A) that is assembled from the sodium(I) nodes and μ-H_2L^- linkers. Topological analysis of the simplified 1D underlying chains (Figure 4B) reveals a uninodal 2-connected net with the 2C1 topology. In the crystal packing pattern, the adjacent chains are interdigitated and have a tooth-like arrangement. Compound **2** features a very complex 3D metal-organic architecture (Figure 5A), which is driven by three types of potassium nodes (K1, K2, K3), two types of organic spacers (μ_4- and μ_5-H_2L^- moieties), as well as additional μ-H_2O linkers. From a topological perspective, such a complex framework can be classified as a pentanodal 4,4,4,4,8-connected net that has a unique topology (Figure 5B). It is described by the point symbol of $(4^3.6^2.8)_3(4^4.6^2)_3(4^7.6^8.8^{13})$, wherein the $(4^3.6^2.8)$, $(4^4.6^2)$, and $(4^7.6^8.8^{13})$ notations correspond to the

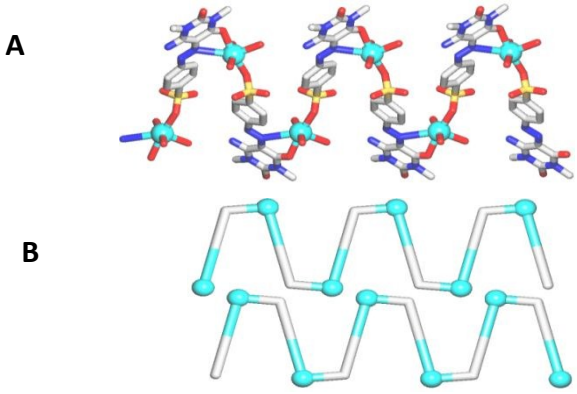

Figure 4. Structural fragments of **1**. (**A**) 1D metal-organic chain along the *a* axis. H atoms are omitted for clarity, color codes: Na (cyan balls), O (red), N (blue), S (yellow), C (gray); (**B**) Topological representation of two tooth-like underlying chains along the *a* axis, showing a 2-connected net with a 2C1 topology. Na nodes (cyan balls), centroids of μ-H_2L^- linkers (gray).

K2/H_2L^-, K3/H_2L^-, and K1(μ-H_2O)K1 nodes, respectively. An unprecedented type of this topology was confirmed by a search of different databases.[33,34,42] The heterometallic Ni(II)/Na(I) compound **3** discloses a 1D coordination polymer structure (Figure 6A). It is assembled from the anionic $[Ni(\mu\text{-}HL)_2]^{2-}$ motifs and cationic $[Na_2(\mu\text{-}H_2O)_2(H_2O)_6]^{2+}$ blocks that are arranged into a stair-like chain. Such chains can be topologically classified as a uninodal 2-connected net with a decorated 2C1 topology (Figure 6B).

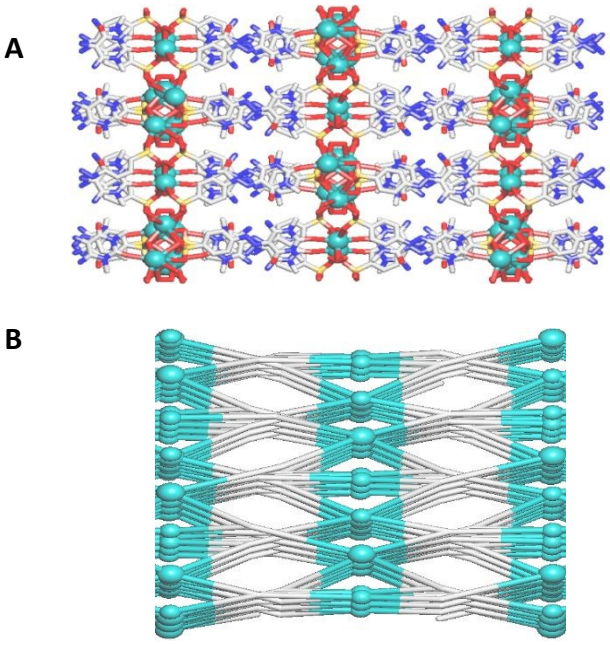

Figure 5. Structural fragments of **2**. (**A**) 3D metal-organic framework along the *c* axis. H atoms are omitted for clarity, color codes: K (turquoise balls), O (red), N (blue), S (yellow),

C (gray); (**B**) Topological representation of the 3D underlying net showing a pentanodal 4,4,4,4,8-connected framework with the unique topology. K2 and K3 nodes (smaller turquoise balls), centroids of K1(μ-H_2O)K1 nodes (larger turquoise balls), centroids of μ_4- and μ_5-H_2L^- nodes (gray).

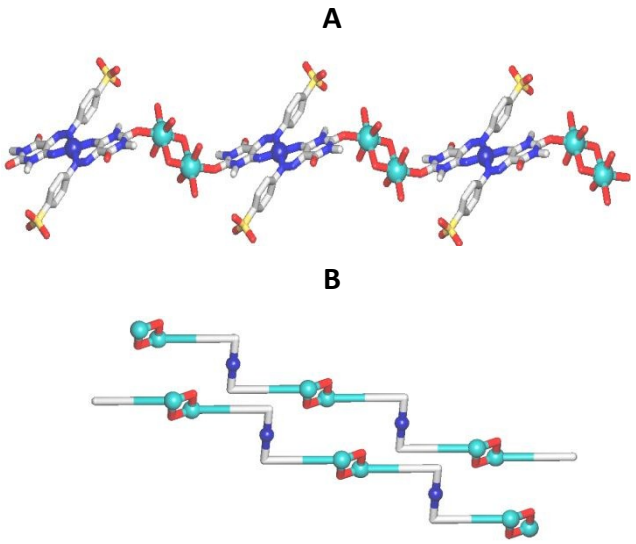

Figure 6. Structural fragments of **3**: (**A**) 1D metal-organic chain along the *a* axis. H atoms are omitted for clarity, color codes: Ni (blue balls), NaK (turquoise balls), O (red), N (blue), S (yellow), C (gray); (**B**) Topological representation of two stairs-like underlying chains along the *a* axis showing a 2-connected net with a decorated 2C1 topology. K nodes (turquoise balls), Ni nodes (blue balls), centroids of μ-HL^{2-} linkers (gray), centroids of μ-H_2O linkers (red).

Theoretical study

The theoretical study was devoted to an analysis of the π-π stacking interactions observed in the solid state architectures of compounds **1** and **2**, which are very relevant for the crystal packing. We have particularly focused our attention to the influence of the coordination of the ligand to Na and K upon the π-stacking interaction. At first, the molecular electrostatic energy (MEP) surfaces of the ligand and its sulfonate sodium salt have been computed to rationalize the interaction from an electrostatic point of view (see Figure 7). In the free ligand (H_3L, Figure 7a), the MEP values over the two six membered rings are +19 kcal/mol (aminouracil ring) and –9.5 kcal/mol (*p*-sulfonate phenyl ring). Therefore, one ring of the ligand is electron deficient (π-acidic) and the other one is electron rich (π-basic), thus anticipating a strong ability to establish antiparallel π-stacking interactions, which are electrostatically

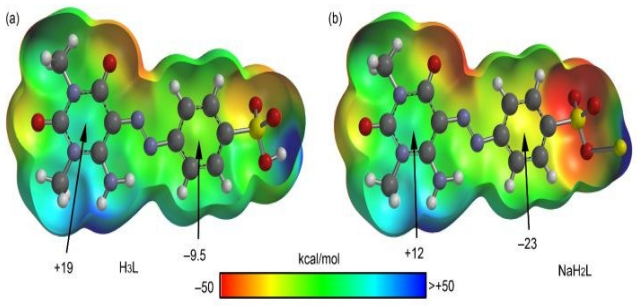

Figure 7. Molecular electrostatic potential (MEP) surfaces of the H_3L ligand and its sodium salt (NaH_2L). The isosurface value is 0.001 a.u. The MEP energies at selected points of the surface have been indicated in kcal/mol.

very favoured. The MEP surface of the sodium salt (Na-H_2L, see Figure 7b) shows a similar behaviour exhibiting π-acidic and π-basic rings. However, the MEP value over the aminouracil ring decreases to +12 kcal/mol (less π-acidic) and that over the *p*-sulfonatephenyl ring becomes more negative (more π-basic, –23 kcal/mol). In Figure 8a we represent a partial view of the X-ray packing of compound **1** where the formation of the antiparallel π-stacking interactions is indicated. Since the structure is polymeric, we have used a theoretical model where two methanesufonate ligands have been used (see small arrows in Figure 8b). First of all, we have studied energetically the formation of this π-stacked dimer (model of the X-ray structure), which is very favorable ΔE_1 = –34.4 kcal/mol in agreement with the MEP analysis (donor-acceptor interaction). This large interaction energy confirms the importance of the interaction in the solid state, likely adjusting the final geometry of 3D polymer. We have studied the effect of the ligand coordination to Na on the π-stacking energy by computing two additional models. First, we have analysed the effect of eliminating the Na atom that is coordinated by the uracil ring (see Figure 8c); the resulting interaction energy is slightly reduced to ΔE_2 = –33.1 kcal/mol. This indicates a small influence of the Na-coordination on the strength of the π-stacking interaction. Finally, we have eliminated the sodium atom that is bound to the sulfonate group and added an H-atom (see small arrow in Figure 8d) to keep the model neutral. The resulting interaction energy is ΔE_3 = –34.0 kcal/mol, thus indicating a negligible influence of the Na-coordination on the dimerization energy.

In Figure 9a we represent a partial view of the X-ray packing of compound **2** where the formation of an infinite 1D column with antiparallel π-stacking interactions is established. Since the structure of **2** is also polymeric, we have used a theoretical model as represented in Figure 9b), where ligand is mono-coordinated to K. The formation of this π-stacked dimer is significantly stronger ΔE_4 = –59.5 kcal/mol than that computed for compound **1**. This is likely due to the different π-stacking mode observed in **2**, where the overlap between the acidic π-system and the electron rich π-sulfonate-phenyl ring is excellent. The overlap is facilitated by the fact that in compound **2** the ligand is not coordinated to the metal via the N-atom of the azo group. We have also studied the effect of the K coordination on the π-stacking energy. In Figure 9c we represent an additional model where the K atoms have been substituted by H atoms. As a result, the interaction energy is significantly reduced to ΔE_5 = –52.4 kcal/mol, thus indicating that the ligand coordination to K reinforces the π-stacking interactions.

We have also computed the "Noncovalent Interaction plot" (NCIplot) index in order to further characterize the antiparallel π-stacking interactions in the dimers of compounds **1** and **2**. The NCIplot is an intuitive visualization index that enables the identification of non-covalent interactions easily and efficiently.

The NCIplot is convenient to analyse host–guest interactions since it clearly shows which molecular regions interact. The colour scheme is a red-yellow-green-blue scale with red (repulsive) and blue (attractive). Yellow and green surfaces correspond to weak repulsive and weak attractive interactions, respectively. The representations of the NCIplot index for both compounds are shown in Figure 10. The NCIplot reveals the existence of a green and extended isosurface between the π-systems of the organic ligands in both compounds, thus characterizing the π–π interaction. Interestingly, in compound **2** the isosurface is clearly more extended and completely embraces both rings and the azo linker. The shape of the NCIplot isosurfaces agrees well with binding energies commented above for compounds **1** and **2**.

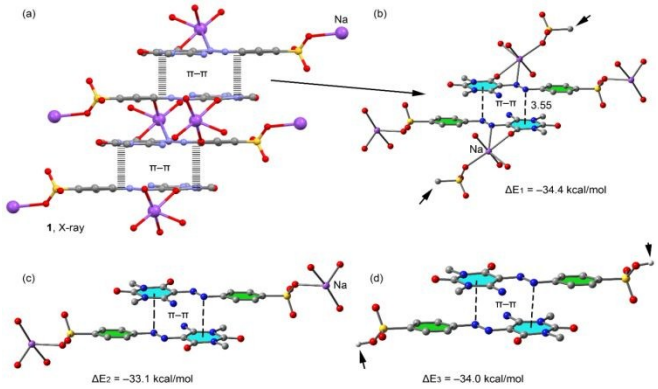

Figure 8. (a) Partial view of the X-ray solid state structure of **1**. H-atoms omitted for clarity. (b-d) Theoretical models used to evaluate the interaction energy. Distances in Å. H-atoms omitted for clarity apart from those belonging to the sulfonic acid.

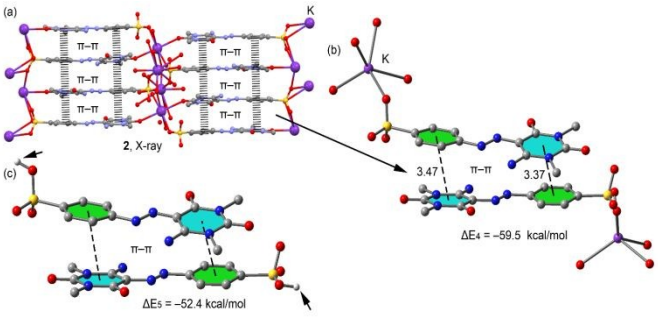

Figure 9. (a) Partial view of the X-ray solid state structure of **2**. H-atoms omitted for clarity. (b,c) Theoretical models used to evaluate the interaction energy. Distances in Å. H-atoms omitted for clarity apart from those belonging to the sulfonic acid.

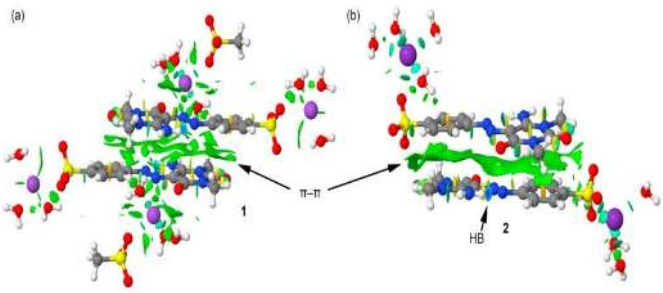

Figure 10. NCI surfaces of the dimer of compounds **1** (a) and **2** (b). The gradient cut-off is s = 0.35 au, and the color scale is −0.04 < ρ < 0.04 au.

Solution behavior: NMR and UV-vis studies

It is evident that the solid state monoazo derivatives of 1,3-dimethyl-6-aminouracil exist in hydrazone form in solution, whereas their Ni(II) complexes are in the azo-form both in solution and solid state.[28] The ^{1}HNMR spectra in DMSO-D_6 of **1-3** are given in Figure S6 and S7 (ESI). The compounds **1** and **2** exist in hydrazone form in solution and show the hydrazone (=N-NH-) and imine (=NH-) proton signals at 11.79 & 11.77 (Figure S6A) and 8.71 & 8.74 ppm (Figure S7), respectively. In compound **3** (Figure S6B), these two proton signals are absolutely absent; instead, a coordinated deprotonated amino (-HN→) proton signal (broad) appears at 4.62 ppm and supports that it exists in azo-form, as in the solid state, with a square-planar $[Ni(HL)_2]^{2-}$ unit. The other protons are in usual positions.[28] The ^{13}C NMR signals of the compounds **1**–**3** are also concomitant with the reported values (Figures S8–S10, ESI).

The UV-vis spectra of **1**–**3** were recorded in different solvents including MeOH, EtOH, DMF, and DMSO (Figures S11-S13, ESI). The spectra of **1** and **2** show a broad absorption band (363 nm - 373 nm) for overlapping π→π* and n→π* transitions,[28] and a weak band at 270 nm for π→π* transition of the aromatic moiety. Compound **3** exhibits three well defined bands at 271, 334, and 423-439 nm, as well as a weak shoulder centered at 580 nm. The longer wavelength bands could be attributed to an intra–ligand charge transfer (ILCT) transition.[28c,f] Thus, the solution studies evidence that the CPs, **1**-**3** disaggregate in the solution to produce simple molecular units.

Electrical conductivity

Solid state low frequency electrical conductivity of the compounds **1**–**3** was measured by impedance spectroscopy. This method represents a well established technique used for evaluating electrical conductivity (σ) of a material. The Nyquist plots of the real and the imaginary parts of the complex impedance (Z) as a function of frequency (ω) were built up over a 20 Hz –1 MHz range of frequency, using the conductivity data of all compounds (Figure 11A–C). Moreover, the maximum real *Z′* value represents the contribution of combined series and parallel resistances to the capacitor. Hence, the equivalent circuit of the device can be represented by a single parallel resistor *Rp* and capacitor *Cp* network with a series resistance *Rs*, as shown in the Figure 11D. The impedance spectra for **2** and **3** (Figures 11B–C) are semicircles, whereas it is a part of semicircle for **1** (Figure 11A). The intercept of semicircle on the real *Z′* axis expresses the bulk resistance of a material. Accordingly, it is primarily suggested that the compound **1** (Na 1D–CP) is a better conducting material (shows lower resistance) than the compounds **2** and **3**. Thereafter, the impedance spectra have been fitted using the following equation,[39] Eq. 1.

$$Z = R_s + \frac{R_p}{1 + (j\omega R_p C_p)^{\alpha}} \qquad (1)$$

Herein, the exponent α is a distribution of relaxation times and ω is the angular frequency. The fitted curves are well matched with the experimental plots (Figures 11A–C), indicating a

narrow distribution of relaxation times with the least dielectric loss. The fitted values from the impedance spectra could be used for evaluating low frequency impedance data (*i.e.*, Z(0) = R_S + R_P; resistance of the device). The R_S values (alternatively called the contact resistance between the compound and the electrode interface) of the compounds are 1.08×10^3 ohm for **1**, 32.99×10^3 ohm for **2**, and 484.01×10^3 for **3**.

The dielectric property of the compounds as a function of frequency at room temperature was then evaluated. Like R_S, the impedance data could be used to calculate the frequency responsive real (ε′) and imaginary (ε″) parts of the dielectric constants of the compounds, using the following equations[41] (Eqs. 2 and 3). The symbols A, d, and ε_0 are denoted as the device area (3.0×10^{-4} m^2), sample thickness (3.0×10^{-3} m), and permittivity in vacuum.

$$\varepsilon' = \frac{Im\,Z}{\frac{\omega\epsilon_0 A}{d}|Z|^2} \qquad (2)$$

$$\varepsilon'' = \frac{Real\,Z}{\frac{\omega\epsilon_0 A}{d}|Z|^2} \qquad (3)$$

The plots of real part of dielectric constant (ε′) *vs.* frequency of the compounds are shown in Figure 12A. The low frequency dielectric constant of the compound **1** is 7.4×10^5 at 20 Hz which is ~60 times greater than that of the compound **2** (1.18×10^4) and is negligible for compound **3** (5.4×10^2).

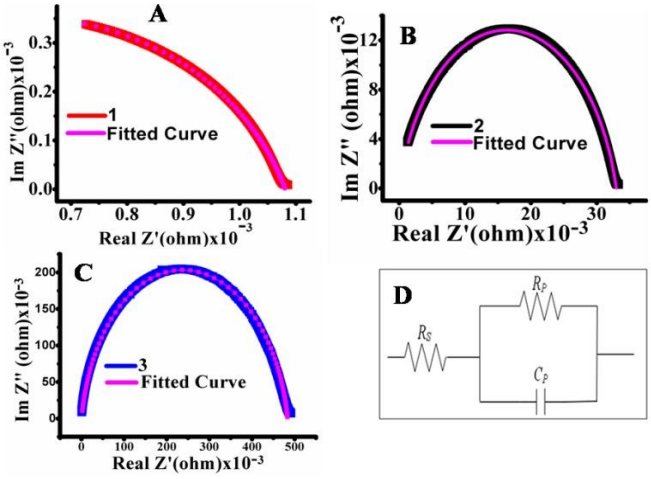

Figure 11. Nyquist plot of impedance(Z), real Z′ *vs* Im Z″ for **1** (A), **2** (B), and **3** (C); circuit diagram (D).

Nevertheless, the dielectric losses could be correlated with the conductivity (σ) of all compounds by the equation,[39] Eq. 4.

$$\sigma^* = j\varepsilon_0\omega\varepsilon^* = j\varepsilon_0\omega(\varepsilon' - j\varepsilon'') = \varepsilon_0\omega\varepsilon'' + j\varepsilon_0\omega\varepsilon' \qquad (4)$$

The real part of σ* is represented as σ_R. The low frequency conductivity (σ_R at 20Hz) of the compounds has been estimated from the σ *vs* frequency plot as depicted in Figure 12B–D and tabulated in Table 2. The σ_R at 20Hz for the compounds **1**, **2**, and **3** are 2.2×10^{-4}, 7.2×10^{-6}, and 4.8×10^{-7} S cm^{-1}, respectively. These values are comparable to those of classic solid-state ion conductors (10^{-3} to 10^{-8} S cm^{-1}).[43] The results evidence that the electrical conductivity of **1** is far greater than that of **2** which is again better conductive than **3**.

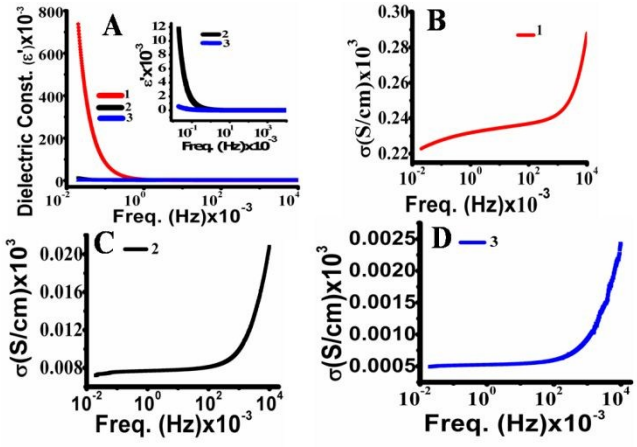

Figure 12. The plots of (**A**) dielectric loss with frequency (Hz); (**B**-**D**) conductivity vs frequency for the compounds **1** (B), **2** (C), and **3** (D).

Table 2. Conductivity data for **1**–**3**.

Compound	R_S (ohm)	ε′ at 20 Hz	σ_R, S cm^{-1} at 20 Hz
1	1.08×10^3	7.4×10^5	2.2×10^{-4}
2	32.99×10^3	1.18×10^4	7.2×10^{-6}
3	484.01×10^3	5.4×10^2	4.8×10^{-7}

The conductivity data of the compounds **1**–**3** can be correlated with the coordination modes of the sulfonate group of the ligand, 1,3-dimethyl-5-(*p*-sulfonate-phenylazo)-6-aminouracil (H_3L). From the structures (Figures 1–3) and conductivity data (Table 2) it can be realized that the binding of the sulfonate group is essential for enhanced conductivity, and the coordination of sulfonate group in a monodentate fashion (compound **1**) is more effective than the multiple bridging mode (compound **2**) or the non-coordination (compound **3**). The order of conductivity in the studied compounds reveals the **1**>>**2**>**3** trend. From the MEP study (Figure 7) it can be seen that the ligand possesses the positive (uracil moiety) and negative (phenyl moiety) potentials in an intramolecular form, which are conjugated *via* the azo (-N=N-) functionality. Given these opposite charges and considering a linkage between sulfonate-O donor and the metal center [Na(I) for **1** and K(I) for **2**], the charge transfer may take place through the conjugated coordination polymers, resulting in the development of conductivity in them. Further theoretical study of the solid state structures **1** and **2** shows that they possess anti-parallel π-π stacking interactions in different modes. In **1**, the uracil moiety (π^+) stacks with the azo (π^-) group, leaving the sulfonated phenyl (π^-) group intact, whereas in **2** the uracil moiety (π^+) stacks with the sulfonated phenyl (π^-) group in anti-parallel manner. Such

types of π-π stacking interactions are generally described as electrostatic in nature that could reduce the conductivity.[19]

There are various reports on conductivity of sulfonated derivatives. Zheng and Zhu[18] measured electrical conductivity at room temperature in the range of $1.2\times10^{-5} - 9.89\times10^{-8}$ S cm^{-1} on the systems composed of silver-sulfobenzoate/N-donor ligands and demonstrated that the Ag-Ag, Ag-π, π-π, and hydrogen bonding interactions lead to the formation multidimensional polymeric networks and play an important role for electron transfer. Wei *et. al.*[20] evaluated the proton conductivity values of sulfonated Cu(II)-based coordination polymers and found the conductivity in the 10^{-2} to 10^{-4} S cm^{-1} range. Noor *et. al.*[19] reported ionic conductivity of ionomers based on polymeric sulfonated derivatives and alkyl-ammonium/sodium salts and demonstrated that the ionic quaternary ammonium cation is necessary to reduce the electrostatic interchain interactions. The electrical conductivity through the polymeric chain in **2**, which has electrostatic force guided π-π stacking interactions in exact anti-parallel manner, may therefore experience more hindrance if compared to **1**. As a consequence, the conductivity of **1** is significantly higher than that of **2**.

4. Conclusions

In the current work, we have assembled and fully characterized two homometallic alkali metal containing coordination polymers derived from a sulfonated monoazo 6-aminouracil derivative (H_3L) as a promising building block. In addition, a related heterometallic Na/Ni coordination polymer has also been generated. All the products **1**–**3** bear the same multifunctional organic spacer and were assembled *in situ* with no need for the isolation of an organic building block (H_3L). The presence of a sulfonate/sulfonic acid group in the ligand and its different coordination modes turns all three compounds to be structurally different. In fact, their structures range from 1D coordination polymers (Na derivative **1** and Na/Ni derivative **3**) to a 3D metal-organic framework (K derivative **2**). The obtained compounds were topologically classified, allowing an identification of a very complex and topologically unique 3D net in **2**. The sulfonate group and one uracil-O donor play a particularly important structure-guiding role, and are responsible for the formation of coordination polymer networks. As an example of functional properties of the obtained compounds, electrical conductivity was studied revealing their semi-conductive nature at room temperature. The conductivity of **1** (2.2×10^{-4} S cm^{-1}) is indeed very promising, indicating that this Na(I) coordination polymer can be considered as a low frequency semiconductor. Besides, all the obtained products represent the first coordination compounds derived from a new multifunctional 6-aminouracil ligand (H_3L) as attested by a search of the Cambridge Structural Database. Apart from this structural novelty, the present work also contributes to the synthesis of new coordination polymers driven by multifunctional ligands that exhibit promising structural, topological and conductivity features.

Conflicts of interest

"There are no conflicts to declare".

Acknowledgements

The authors are thankful to Department of Chemistry, NIT Agartala, India for providing financial support and research facilities; to the MINECO of Spain (project CTQ2014-57393-C2-1-P FEDER funds) for financial support and the CTI for computational facilities; to FCT and Portugal 2020 (LISBOA-01-0145-FEDER-029697, UID/QUI/00100/2013) for financial support. The publication was also prepared with the support of the RUDN University Program 5-100. A.P. greatly acknowledges NIT, Agartala for financial support.

References

1 (*a*) The Chemistry of Metal-Organic Frameworks, 2 Volume Set: Synthesis, Characterization, and Applications, S. Kaskel (Ed), John Wiley & Sons, 2016. (*b*) Metal-Organic Framework Materials, L. R. MacGillivray, C. M. Lukehart (Eds.), John Wiley & Sons, Chichester, U.K., 2014.

2 (*a*) T. A. Fernandes, C. I. M. Santos, V. André, J. Kłak, M. V. Kirillova and A. M. Kirillov, *Inorg. Chem.*, 2016, **55**, 125-135; (*b*) J.Z. Gu, Y. H. Cui, X. X. Liang, J. Wu, D. Y. Lv and A. M. Kirillov, *Cryst. Growth Des.*, 2016, **16**, 4658-4670; (*c*) S. S. P. Dias, M. V. Kirillova, V. André, J. Kłak and A. M. Kirillov, *Inorg. Chem.*, 2015, **54**, 5204-5212; (*d*) S. W. Jaros, M. F. C. G. da Silva, M. Florek, M. C. Oliveira, P. Smoleński, A. J. L. Pombeiro and A. M. Kirillov, *Cryst. Growth Des.*, 2014, **14**, 5408-5417.

3 A. Y. Robin and K. M. Fromm, *Coord. Chem. Rev.*, 2006, **250**, 2127-2157.

4 (*a*) J.-Z. Gu, M. Wen, X. Liang, Z.-F. Shi, M. V. Kirillova and A. M. Kirillov, *Crystals* 2018, **8**, 83; (*b*) Ł. Jaremko, A. M. Kirillov, P. Smoleński and A. J. L. Pombeiro, *Cryst. Growth Des.*, 2009, **9**, 3006-3010; (*c*) M. N. Kopylovich, Y. Y. Karabach, K. T. Mahmudov, M. Haukka, A. M. Kirillov, P. J. Figiel and A. J. L. Pombeiro, *Cryst. Growth Des.*, 2011, **11**, 4247-4252; (*d*) S. S. P. Dias, M. V. Kirillova, V. André, J. Kłak and A. M. Kirillov, *Inorg. Chem. Front.* 2015, **2**, 525-537; (*e*) S. A. Sotnik, R. A. Polunin, M. A. Kiskin, A. M. Kirillov, V. N. Dorofeeva, K. S. Gavrilenko, I. L. Eremenko, V. M. Novotortsev and S. V. Kolotilov, *Inorg. Chem.* 2015, **54**, 5169-5181.

5 (*a*) J. Balzarini, H. Mitsuya, E. De Clercq and S. Broder, *Int. J. Cancer*, 1986, **37**, 451-457; (b) W. H. Ojala, C. R. Ojala and W. B. Gleason, *Antiviral Chem. Chemother.*, 1995, **6**, 25-33.

6 (a) R. I. Brinkworth and D. P. Fairlie, *Biochem. Biophys. Res. Commun.*, 1992, **188**, 624-630; (b) H. Sun, Y. Liu, C. Zhang, X. Luo and X. Jiang, *Anal. Methods*, 2017, **9**, 1185-1189

7 J. Schartner, A. Nabers, B. Budde, J. Lange, N. Hoeck, J. Wiltfang, C. Kötting and K. Gerwert, *ACS Med. Chem. Lett.*, 2017, **8**, 710–714.

8 S. Sellarajah, T. Lekishvili, C. Bowring, A. R. Thompsett, H. Rudyk, C. R. Birkett, D. R. Brown and I. H. Gilbert, *J. Med. Chem.*, 2004, **47**, 5515-5534.

9 Y. Yang, M. Cui, X. Zhang, J. Dai, Z. Zhang, C. Lin, Y. Guo and B. Liu, *J. Med. Chem.*, 2014, **57**, 6030–6042.

10 (a) A. W. Hanson, *Acta Cryst.*, 1973, **B29**, 454-460; (b) K. Horita and M. Satake, *Analyst*, 1997, **122**, 1569-1574.

11 (a) H.-X Chen, F. Zhou, Y. Ma, X.–P. Xu, J.–F. Ge, Y. Zhang, Q.–F. Xu and J.–M. Lu, *Dalton Trans*, 2013, **42**, 4831-4839; (b) J. Lü, S.–Y. Gao, J.–X. Lin, L.–X. Shi, R. Cao and S. R. Batten, *Dalton Trans*, 2009, 1944-1953; (c) F. A. Rad, Z. Rezvani and F. Khodam, *RSC Adv.*, 2016, **6**, 11193-11203.

12 (*a*) H. Bock, J.-M. Lehn, J. Pauls, S. Holl and V. Krenzel, *Angew.Chem., Int. Ed.*, 1999, **38**, 952-955; (*b*) L. Zhang, P. Cheng, L.-F. Tang, L.-H. Weng, Z.-H. Jiang, D.-Z. Liao, S.-P. Yan and G.-L. Wang, *Chem. Commun.*, 2000, 717-718.
13 (*a*) A. R. Kennedy, M. P. Hughes, M. L. Monaghan, E. Staunton, S. J. Teat and W. E. Smith, *J. Chem. Soc. Dalton Trans.*, 2001, 2199–2205; (*b*) A. R. Kennedy, J. B. A. Kirkhouse, K. M. McCarney, O. Puissegur, W. E. Smith, E. Staunton, S. J. Teat, J. C. Cherryman and R. James, *Chem. Eur. J.*, 2004, **10**, 4606-4615.
14 A. R. Kennedy, J. B. A. Kirkhouse and L. Whyte, *Inorg. Chem.*, 2006, **45**, 2965-2971.
15 C. Astbury, L. K. Conway, C. Gillespie, K. Hodge, E. Innes and A. R. Kennedy, *Dyes Pigm.*, 2013, **97**, 100-104.
16 (*a*) A. P. Côté and G. K. H. Shimizu, *Chem. Commun.*, 2001, 251–252; (*b*) S. A. Dalrymple and G. K. H. Shimizu, *Chem. Eur. J.*, 2002, **8**, 3010–3015.
17 H.-X. Chen, F. Zhou, Y. Ma, X.-P. Xu, J.-F. Ge, Y. Zhang, Q.-F. Xu and J.-M. Lu, *Dalton Trans.*, 2013, **42**, 4831-4839.
18 X.-F. Zheng and L.-G. Zhu, *Inorg. Chim. Acta* 2011, **365**, 419–429.
19 (*a*) S. A. M. Noor, J. Sun, D. R. MacFarlane, M. Armand, D. Gunzelmann and M. Forsyth, *J. Mater. Chem. A*, 2014, **2**, 17934-17943; (*b*) S. A. M. Noor, D. Gunzelmann, J. Sun, D. R. MacFarlaneac and M. Forsyth, *J. Mater. Chem. A*, 2014, **2**, 365-374.
20 (*a*) M. Wei, J. Fu, Y. Wang, Y. Zhang, H. Zang, K. Shao, Y. Li and Z. Su, *CrystEngComm.*, 2017, **19**, 7050-7056; (*b*) M. Wei, J. Fu, Y. Wang, J. Gu, B. Liu, H. Zang, E. Zhou and K. Shao, Z. Su, *J. Mater. Chem. A*, 2017, **5**, 1085-1093.
21 K. West, L. Bay, M. M. Nielsen, Y. Velmurugu and S. Skaarup, *J. Phys. Chem. B*, 2004, **108**, 15001-15008.
22 A. J. Oostra, K. H. W. van den Bos, P. W. M. Blom and J. J. Michels, *J. Phys. Chem. B*, 2013, **117**, 10929−10935.
23 R. Rondla, J. C. Y. Lin, C. T. Yang and I. J. B. Lin, *Langmuir*, 2013, **29**, 11779−11785.
24 L. Zhang, J. M. Cole and C. Dai, *ACS Appl. Mater. Interfaces*, 2014, **6**, 7535−7546.
25 C. Qin, Y. Feng, W. Luo, C. Cao, W. Hu and W. Feng, *J. Mater. Chem. A*, 2015, **3**, 16453-16460.
26 M. Bouhdada, M. E.L. Amane and N. E. Hamzaoui, *Inorg. Chem. Commun.*, 2019, **101**, 32-39.
27 V. G. Vidya, V. Sadasivan, S. S. Meena and P. Bhatt, *Orient. J. Chem.*, 2018, **34**, 45-54.
28 (*a*) D. Debnath, S. Roy, B.-H. Li, C.-H. Lin and T. K. Misra, *Spectrochim. Acta*, 2015, **140A**, 185-197; (*b*) D. Debnath, A. Purkayastha, R. Choudhury and T. K. Misra, *Ind. Chem. Soc.*, 2016, **93**, 989-998; (*c*) D. Debnath, A. Purkayastha, R. Choudhury and T. K. Misra, *J. Chin. Chem. Soc.*, 2016, **63**, 580-589; (*d*) D. Debnath, A. Purkayastha, A. M. Kirillov, R. Ganguly and T. K. Misra, *J. Mol. Struct.*, 2017, **1150**, 118-126; (*e*) A. Purkayastha, D. Debnath, S. Roy, A. Bauzá, R. Choudhury, A. Frontera and T. K. Misra, *Eur. J. Inorg. Chem.*, 2016, **36**, 5585-5593; (*f*) D. Debnath, S. Roy, A. Purkayastha, A. Bauzá, R. Choudhury, R. Ganguly, A. Frontera and T. K. Misra, *J. Mol. Struct.*, 2017, **1141**, 225-236; (*g*) A. Purkayastha, D. Debnath, R. Ganguly and T. K. Misra, *J. Chem. Crystallogr.*, 2017, **47**, 101-109; (*h*) A. Purkayastha, A. Frontera, R. Ganguly and T. K. Misra, *J. Mol. Struct.*, 2018, **1170**, 70-81; (*i*) A. Purkayastha, D. Debnath, M. Majumdar, J. Ortega-Castro, A. M. Kirillov, R. Ganguly, J. Klak, A. Frontera and T. K. Misra, *Inorg. Chim. Acta*, 2018, **482**, 384-394.
29 SAINT, Data Reduction and Frame Integration Program for the CCD Area-Detector System. Bruker Analytical X-ray Systems, Madison, Wisconsin, USA, 1997–2006.
30 G. M. Sheldrick, SADABS, Program for Area Detector Adsorption Correction, Institute for Inorganic Chemistry, University of Göttingen, Göttingen, Germany, 1996.
31 O. V. Dolomanov, L. J. Bourhis, R. J. Gildea, J. A. K. Howard and H. Puschmann, OLEX2, *J. Appl. Cryst.*, 2009, **42**, 339-341.
32 G. M. Sheldrick, *Acta Cryst.*, 2015, **C71**, 3-8.
33 (*a*) V. A. Blatov, *IUCr CompComm Newslett.*, 2006, **7**, 4-38; (*b*) V. A. Blatov, A. P. Shevchenko and D. M. Proserpio, *Cryst. Growth Des.*, 2014, **14**, 3576-3586.
34 (*a*) M. O'Keeffe and O. M. Yaghi, *Chem. Rev.*, 2012, **112**, 675-702; (*b*) M. Li, D. Li, M. O'Keeffe and O. M. Yaghi, *Chem. Rev.*, 2014, **114**, 1343-1370.
35 M. J. Frisch, G. W. Trucks, H. B. Schlegel, G. E. Scuseria, M. A. Robb, J. R. Cheeseman, G. Scalmani, V. Barone, B. Mennucci, G. A. Petersson, H. Nakatsuji, M. Caricato, X. Li, H. P. Hratchian, A. F. Izmaylov, J. Bloino, G. Zheng, J. L. Sonnenberg, M. Hada, M. Ehara, K. Toyota, R. Fukuda, J. Hasegawa, M. Ishida, T. Nakajima, Y. Honda, O. Kitao, H. Nakai, T. Vreven, J. A. Montgomery, Jr., J. E. Peralta, F. Ogliaro, M. Bearpark, J. J. Heyd, E. Brothers, K. N. Kudin, V. N. Staroverov, R. Kobayashi, J. Normand, K. Raghavachari, A. Rendell, J. C. Burant, S. S. Iyengar, J. Tomasi, M. Cossi, N. Rega, J. M. Millam, M. Klene, J. E. Knox, J. B. Cross, V. Bakken, C. Adamo, J. Jaramillo, R. Gomperts, R. E. Stratmann, O. Yazyev, A. J. Austin, R. Cammi, C. Pomelli, J. W. Ochterski, R. L. Martin, K. Morokuma, V. G. Zakrzewski, G. A. Voth, P. Salvador, J. J. Dannenberg, S. Dapprich, A. D. Daniels, Ö. Farkas, J. B. Foresman, J. V. Ortiz, J. Cioslowski, and D. J. Fox, Gaussian 09 (Gaussian, Inc., Wallingford CT, 2009).
36 S. Grimme, J. Antony, S. Ehrlich and H. Krieg, *J. Chem. Phys.*, 2010, **132**, 154104.
37 S. F. Boys and F. Bernardi, *Mol. Phys.*, 1970, **19**, 553–566.
38 J. Contreras-García, E. R. Johnson, S. Keinan, R. Chaudret, J. -P. Piquemal, D. N. Beratan and W. Yang, *J. Chem. Theory Comput.*, 2011, **7**, 625-632.
39 S. P. Mondal, R. Aluguri and S. K. Ray, *J. Appl. Phys.*, 2009, **105**, 114317.
40 B. V. S. K. Rao, K. Chandra Mouli, N. Rambabu, A. K. Dalai and R. B. N. Prasad, *Catal. Commun.*, 2011, **14**, 20-26.
41 G. Mezei and R. G. Raptis, *New J. Chem.*, 2003, **27**, 1399-1407.
42 The Cambridge Structural Database: C. R. Groom, I. J. Bruno, M. P. Lightfoot and S. C. Ward, *Acta Cryst.*, 2016, **B72**, 171-179.
43 P. Colomban, A. Novak, in Proton Conductors: Solids, Membranes and Gels (Materials and Devices), ed. P. Colomban, Cambridge University Press, Cambridge, 1992, pp. 38–60.